3D reconstruction of particle agglomerates using multiple scanning electron microscope stereo-pair images

Töberg, Stefan, Reithmeier, Eduard

Stefan Töberg, Eduard Reithmeier, "3D reconstruction of particle agglomerates using multiple scanning electron microscope stereo-pair images," Proc. SPIE 10819, Optical Metrology and Inspection for Industrial Applications V, 108190I (6 November 2018); doi: 10.1117/12.2502485

SPIE.

Event: SPIE/COS Photonics Asia, 2018, Beijing, China

3D reconstruction of particle agglomerates using multiple scanning electron microscope stereo-pair images

Stefan Töberg[a] and Eduard Reithmeier[a]

[a]Institute of Measurement and Automatic Control, Leibniz Universität Hannover, Nienburger Str. 17, 30167 Hannover, Germany

ABSTRACT

Scanning electron microscopes (SEM) allow a detailed surface analysis of a wide variety of specimen. However, SEM image data does not provide depth information about a captured scene. This limitation can be overcome by recovering the hidden third dimension of the acquired SEM micrographs, for instance to fully characterize a particle agglomerate's morphology. In this paper, we present a method that allows the three-dimensional (3D) reconstruction of investigated particle agglomerates using an uncalibrated stereo vision approach that is applied to multiple stereo-pair images. The reconstruction scheme starts with a feature detection and subsequent matching in each pair of stereo images. Based on these correspondences, a robust estimate of the epipolar geometry is determined. A following rectification allows a reduction of the dense correspondence problem to a one-dimensional search along conjugate epipolar lines. So the disparity maps can be obtained using a dense stereo matching algorithm. To remove outliers while preserving edges and individual structures, a disparity refinement is executed using suitable image filtering techniques. The investigated specimen's qualitative depth's information can be directly calculated from the determined disparity maps. In a final step the resulting point clouds are registered. State-of-the-art algorithms for 3D reconstruction of SEM micrographs mainly focus on structures whose image pairs contain hardly or even none-occluded areas. The acquisition of multiple stereo-pair images from different perspectives makes it possible to combine the obtained point clouds in order to overcome occurring occlusions. The presented approach thereby enables the 3D illustration of the investigated particle agglomerates.

Keywords: uncalibrated 3D reconstruction, scanning electron microscopy, multiple stereo-pair images, dense matching, point cloud registration

1. INTRODUCTION

SEM are suitable tools for surface structure analysis, material characterization and the investigation of a large variety of specimen. The process of scanning a specimen in the SEM and using the detected signals for imaging purposes projects the 3D surface structure onto a two-dimensional (2D) image plane. To obtain images that maintain more detailed information about the surface morphology usually low acceleration voltages up to 5 kV are used.[1] Although these images allow for a detailed 2D analysis, no information about the depth is provided. Regarding the morphology of agglomerated or aggregated particle structures, information about the 3D shape are often indispensable for an extensive analysis.

In the last decades 3D reconstruction based on SEM images was a widely addressed topic in scientific researches. The necessity of measuring the 3D surface profiles of structures and objects in the micro- and nanoscale has become a very important task f.i. in the fields of morphological particle characterization[2] or the height inspection of semi conductor components.[3] To overcome the 2D limitation, different concepts have been developed that can basically be divided into photogrammetric and photometric reconstruction methods. The photometric method is based on images taken by symmetrically placed detectors around the beam axis. From these images the gradient information of the surface is estimated and subsequently the surface topography can be computed

Further author information: (Send correspondence to Stefan Töberg)
Stefan Töberg: E-mail: stefan.toeberg@imr.uni-hannover.de, Telephone: +49 511 762 4284

Optical Metrology and Inspection for Industrial Applications V, edited by Sen Han, Toru Yoshizawa, Song Zhang, Proc. of SPIE Vol. 10819, 108190I · © 2018 SPIE
CCC code: 0277-786X/18/$18 · doi: 10.1117/12.2502485

via numerical integration.[4] The main drawback of this method is that its functionality is strongly limited by discontinuities of the surface topography. In contrast photogrammetric methods use several images of the same scene taken from different perspectives that are called stereo images. The detection of corresponding points in two or more images that are a projection of the same 3D object point allows for a reconstruction of the point's 3D location. There are different ways of reconstructing the depth of these corresponding points. Traditional multi-view stereo methods are based on a sparse reconstruction of corresponding feature points.[5] The depth related to each point correspondence can be metrically computed by triangulation techniques provided the camera poses of the different views are known. However, the SEM offers a method to reconstruct the depth using a pair of uncalibrated stereo images.[6] Especially when a truly metric reconstruction is not necessary, it was demonstrated that qualitative reconstruction methods can provide 3D data that allows an advanced illustration and investigation of a surface structure's 3D properties.[7] So far this procedure has only been applied to single stereo images capturing continous surfaces where no large length-to-height ratios were present. However, in some cases one pair of stereo images is not sufficient to capture the whole body of a specimen and some parts stay occluded. Therefore the obtained point clouds from several stereo-pair images are combined to increase the amount of reconstructed surface structure so that the investigated particle's 3D surface morphology can be illustrated. After outlining the algorithms used in the stereo pipeline, the method to register the individually reconstructed point clouds from multiple stereo images is introduced and subsequently the results are demonstrated.

2. STEREO IMAGE ACQUISITION

The quality of the acquired stereo images plays a decisive role in the reconstruction of accurate 3D data. To obtain SEM images that are captured by slightly different perspectives the specimen is tilted via a mechanical stage. This procedure is identical with moving a camera around an object like demonstrated in Fig. 1. Providing that the stage and scan rotation, which is equivalent to the rotation of the image plane around the optical axis, are ideally adjusted, the tilting axis lies in the specimen's surface parallel to the image's v-axis as shown in Fig. 1. The resulting eucentric tilt only causes a horizontal movement of scene points while the eucentric point in the image's center keeps its lateral and vertical position. Under real conditions, these ideal settings usually can't be found and so the eucentric point has to be readjusted after a tilting process. The quality of this readjustment is important to maintain the same focus plane and center point in both stereo images. This leads to a higher degree of similarity between the images that has a positive impact on the reconstruction algorithms. In addition a minimization of the vertical and rotational movements between the stereo-pair images improves the results of the rectification procedure described in Sec. 3.2.

3. 3D RECONSTRUCTION METHODS

In this section the methods of the implemented stereo pipeline are outlined. Starting with the detection of feature points and the robust estimation of the fundamental matrix, an uncalibrated rectification is performed

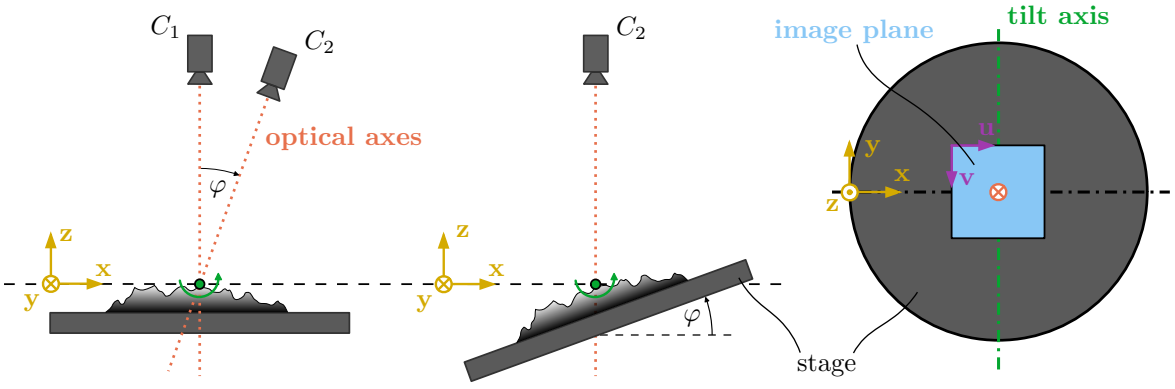

Figure 1. Stereo image acquisition using the equivalence of camera motion (left) and specimen motion (middle) tilting the SEM stage eucentrically. Adjustment of the scan rotation and image plane (right) so that the image's v-axis is parallel to the tilt-axis.

that allows a reduction of the dense correspondence problem to a one-dimensional search along conjugate epipolar lines. This allows to obtain the disparity maps between the rectified image pairs using a dense matching algorithm. Subsequently the disparity maps are postprocessed and the depth is determined pixelwise.

3.1 Epipolar geometry

The epipolar geometry is the intrinsic projective geometry between two stereo-pair images. It is represented by the fundamental matrix F that is a 3×3 matrix of rank 2. If a 3D point M is imaged in the first view as m and m' in the second one, then these image points satisfy the epipolar constraint

$$m'^T F m = 0\,. \tag{1}$$

Considering image noise, the detected correspondences can't fully satisfy this condition what results in an error distance between a point m and the epipolar line $l = F^T m'$. To determine an estimate of the epipolar geometry, it is necessary to find corresponding points in the two stereo images. This problem can be solved automatically using feature detection algorithms that extract characteristical keypoints in an image. Suitable algorithms are f.i. SIFT[8] and KAZE[9] that allow for a robust and precise detection of keypoints in SEM images. To perform a matching between the detected keypoints, a descriptor is assigned to every keypoint that describes its surrounding area. A suitable choice for the SEM images is the SIFT descriptor that is based on the local image gradients and is robust towards rotation and illumination changes. Although the performance of the SIFT and KAZE detectors are comparable, the combination of the KAZE detector and the SIFT descriptor was chosen because it produced slightly better results in the used images. To obtain a first set of matched point correspondences the euclidean distance between the descriptors is computed using a brute force approach. The minimum distance is considered as the best match. By comparing the ratio of the two best matches with a threshold, only high qualitative matches are considered as inliers. Nevertheless this set of correspondences still contains outlier matches that can't be used to compute the fundamental matrix. Therefore an initial estimate of the fundamental matrix is determined using the normalized eight-point algorithm[10] embedded in a robust computation routine like RANSAC.[11] In this procedure n randomly chosen eight-point sets are used to determine n fundamental matrices. Subsequently a cost function for all point correspondences and every fundamental matrix is computed. Based on a chosen threshold, every point correspondence is classified as an in- or outlier. The point set containing the highest amount of inliers and its corresponding fundamental matrix is selected as the final result. A reliable cost function is the

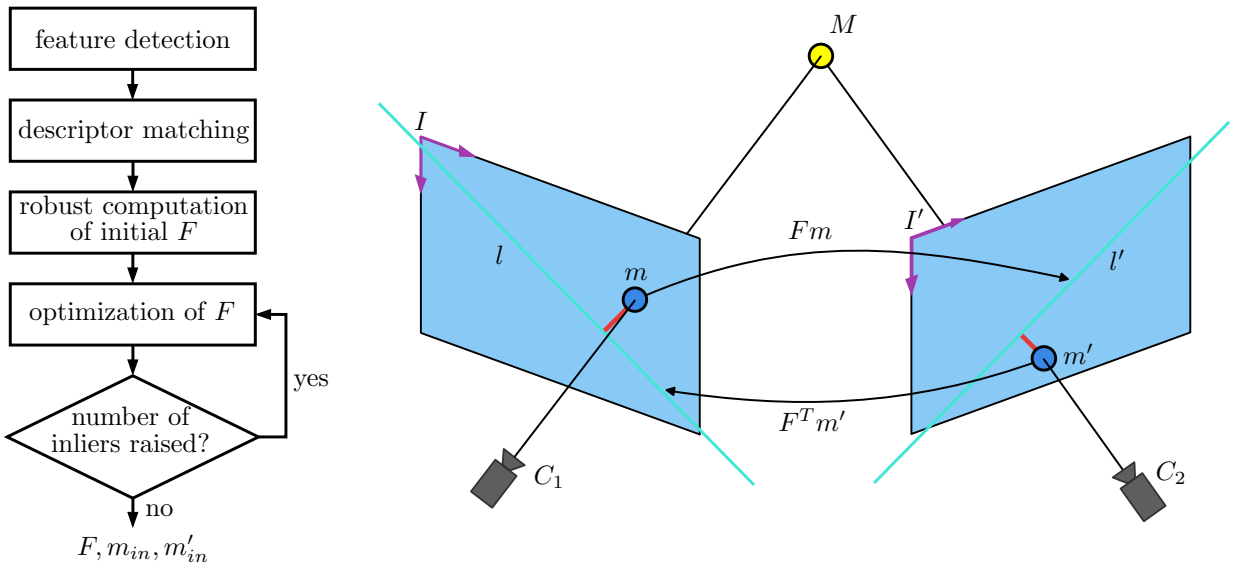

Figure 2. Flow scheme that outlines the determination of the epipolar geometry (left). Illustration of the epipolar geometry describing the relation between a 3D point M and its image points m and m'(right).

sampson distance[12] defined as

$$\sum_i \frac{(m_i'^T F m_i)^2}{(Fx_i)_1^2 + (Fx_i)_2^2 + (F^T x_i')_1^2 + (F^T x_i')_2^2} \tag{2}$$

where $(Fx_i)_j^2$ represents the square of the j-th entry of the vector Fx_i. Eq. (2) gives a close approximation of the reprojection error that can be expressed as the geometric distance $||M_i - \widehat{M}_i||^2 = (m_i - \widehat{m}_i)^2 + (m_i' - \widehat{m}_i')^2$ in that m_i and m_i' are the detected noisy correspondences and $\widehat{m}_i$ and $\widehat{m}_i'$ the true correspondences. In comparision to the in Fig. 2 illustrated distance of a point from its correspondence's projected epipolar line, the sampson distance gives slightly superior results that are almost equal to the ones of the computation expensive reprojection error.[13] The initally estimated fundamental matrix and its related inliers m_{in} and m_{in}' are used as starting values for the minimization of the sampson error that is carried out by the Levenberg-Marquardt (LM) algorithm. This non-linear minimization procedure requires a parametrization of the fundamental matrix that enforces its rank 2 property. A simple choice that works in most scenarios very well is the so called epipolar parametrization[12] that writes the third column of F as a linear combination $f_3 = \alpha f_1 + \beta f_2$ where f_n represents the n-th column of F. After an optimization, the new matrix is used to classify a new set of inliers. As long as the number of inliers rises, this procedure is repeated. If the number of inliers stays constant, the current point set and the related fundamental matrix constitute the final result.

3.2 Uncalibrated Rectification

The objective of a rectification procedure is to transform the stereo-pair images so that between corresponding pixels only a horizontal displacement exists. Given a pair of stereo images and its intrinsic projective geometry in form of the fundamental matrix and its related outlier-free point correspondences, the wanted transformation matrices can be determined using the quasi-euclidean uncalibrated rectification method.[14] Accordingly, the two rectifying transformations H' and H are forced to have the same structure as in the calibrated case satisfying

$$H = KRK^{-1} \qquad\qquad H' = KR'K^{-1} \tag{3}$$

where the matrix K contains the intrinsic parameters of the camera related to the non-rectified image pair with the image center coordinates u_c and v_c as the principal point and f as the unknown focal length in form of

$$K = \begin{pmatrix} f & 0 & u_c \\ 0 & f & v_c \\ 0 & 0 & 1 \end{pmatrix} . \tag{4}$$

Besides the focal length, the two rotation matrices R and R' contain three unknown rotation angles each. Considering that a rotation of a stereo-pair around its baseline that is equal to the x-axes does not affect the rectification, one rotation angle around an x-axis can be set to zero. The remaining six parameters can be determined using an optimization procedure like f.i. the LM algorithm and Eq. (2) as a cost function by combining the Eqs. (1) and (3) to express the fundamental matrix of the non-rectified image pair as

$$F = K^{-1} R'^T F_r R K^{-1} \tag{5}$$

where the fundamental matrix of a rectified image pair F_r has the special form of the skew-symmetric matrix corresponding to the vector $u_1 = (1, 0, 0)$. Although this method usually provides good results, the transformed images can sometimes show a significant amount of distortions. Especially when point correspondences are not evenly spread over the images, these distortions can occur. To check the amount of distortions in the transformed images, the angles of the image corners are computed as a control instance. To determine the four angles, the corners of the transformed images are uniquely detected using a Harris corner detector and the information about each corner's surrounding pixels. The knowledge of the location of the image corners and the connecting vectors subsequently lead to the required angle values. The maximum accepted deviation to a right angle was set to one degree. If this condition is not satisfied, the epipolar geometry is newly determined as described in Sec. 3.1 and the images are rectified again. This procedure is repeated until a satisfying image transformation is obtained that guarantees similar dimensions to the original images.

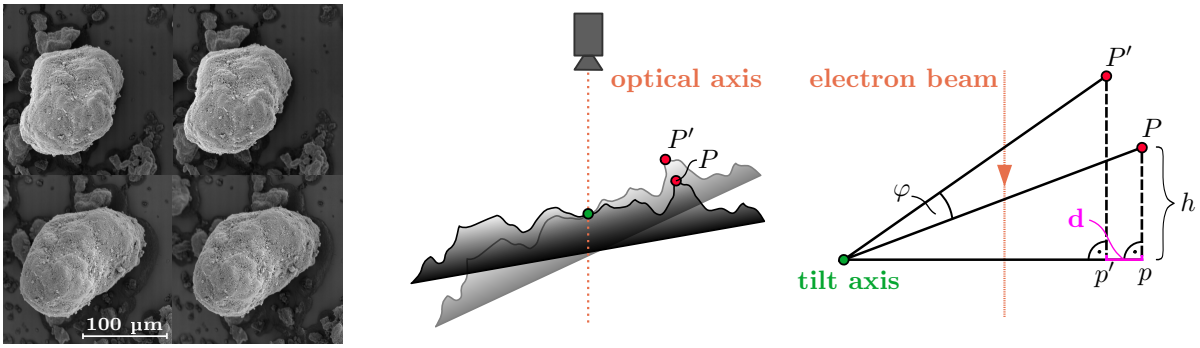

Figure 3. Stereo-pair images of the investigated particles taken with tilt angles of -15°/-10° and 25°/30° (left). Sectional view of a specimen and the movement of a surface point P caused by tilting the SEM stage (middle). Close-up of the resulting triangles formed by the moved surface points and its projections on the reference plane p and p' that are used for the computation of the depth h (right).

3.3 Dense matching and depth computation

After the rectification process, the dense correspondence problem is reduced to a one-dimensional search along conjugate epipolar lines that correspond to the rectified images' u-axes. To obtain a disparity map that contains the pixelwise horizontal displacement between the stereo-pair images, a semi-global block-matching algorithm (SGBM) is used that is based on the famous semi-global matching algorithm.[15] This variation performs an inital subpixel matching using a Birchfield-Tomasi metric[16] and enforces a global smoothness constraint by computing an approximation combining eight symmetrical, one-dimensional pathwise optimizations for each pixel. Subsequently the uniqueness of the processed disparity is checked, comparing the ratio of the computed lowest and highest costs. When the ratio is below a chosen threshold, the pixel is marked as invalid. In addition a left-right consistency check is performed to make sure that correspondences are consistent, marking pixels as invalid if the left-right disparity differs from the right-left disparity by a certain value. These two procedures ensure that occlusions and invalid matches are detected. Finally the obtained disparity maps are post processed using two filtering techniques. The first one is a filter that detects outliers that mostly appear in form of local regions that can be described as speckles. Every pixel of the disparity map acts as a basis for a flood fill algorithm connecting pixels that lie in a defined grey scale range. If the connected part is smaller than a chosen size, the pixels are set to invalid. The second filter is the well-known bilateral filter[17] that is capable of reducing high frequency noise while preserving edges. During the filtering process the invalid pixels are ignored. To prevent an oversmoothing, the filter parameters are selected carefully so that the object's structure is not affected.

The final step of the reconstruction scheme deals with the computaion of the depth. Regarding the fact that the stereo images are rectified and that the imaging system of a SEM can be described by the parallel projection model,[18] the depth h can be computed via

$$h = \frac{dp}{2\sin\frac{\varphi}{2}} \tag{6}$$

where d is the disparity, p the pixel constant of the used magnification and φ the tilt angle.[6] Eq. (6) can be deduced using trignonometric coherences applied to the triangles formed by the tilt axis and the object points P and P' as well as the projected points on the reference plane p and p' that correspond to the dense point matches between the stereo images like illustrated in Fig. 3. For small tilt angles φ, Eq. (6) gives good qualitative results. Although this simplified depth reconstruction can't be considered to be truly metric, the obtained result is suitable to gain access to the specimen's 3D morphological properties.

4. REGISTRATION

In general one pair of stereo images is not sufficient to capture all desired parts of a specimen at once. Especially objects like f.i. the investigated particle agglomerates that tend to have a relatively large height-to-length ratio are difficult to capture from effectively just one view point. A possible solution to this problem is the use

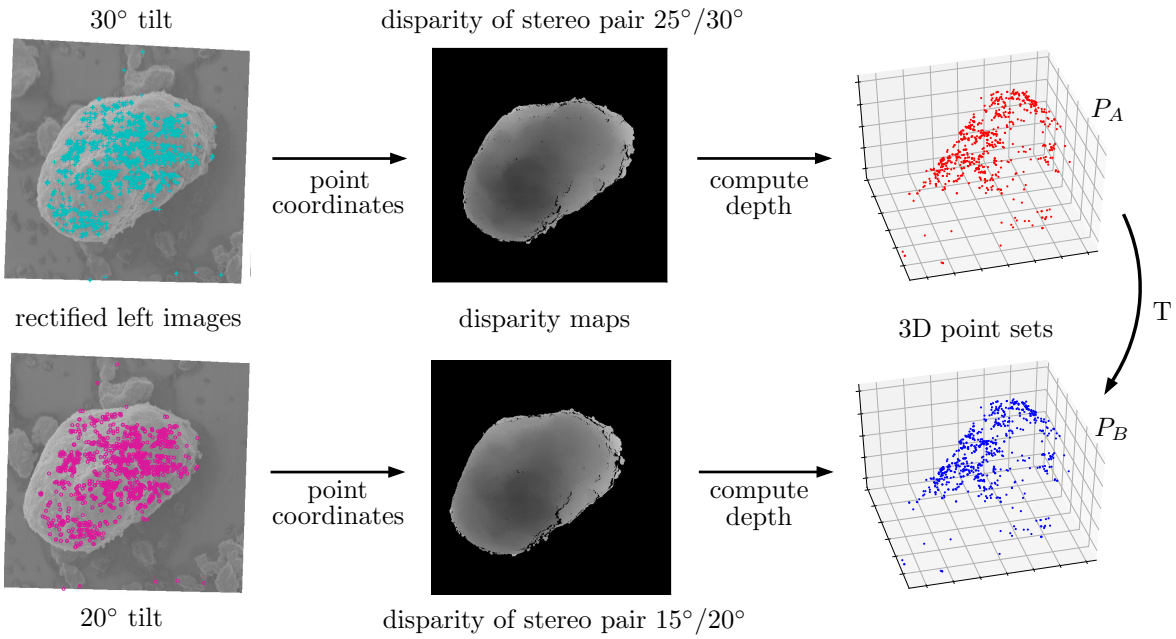

Figure 4. Finding corresponding 3D point sets between individual point clouds using detected and matched features in the rectified left stereo images of two pairs (left), getting the disparity of the matched point coordinates (middle) and computing the depth to obtain the two desired 3D point sets (right).

of multiple stereo images, performing individual 3D reconstructions for every pair and finally registering the obtained point clouds. Due to the fact that the height for every stereo-pair is reconstructed in a local coordinate system, additional information are needed to perform a suitable point cloud alignment.

When a dense matching between two stereo images is performed, for every pixel of the left image, the corresponding pixel in the right image is determined. Therefore the depth reconstruction is based on the left image of a stereo-pair. To create a connection between the 3D reconstructions of different stereo-pair images capturing the same scene, point correspondences between the left images of two stereo-pairs can be computed like explained in section 3.1 provided the angle between the two view points is not too high. The coordinates of the detected point correspondences are then used to assign the corresponding heights of the dense point clouds via the disparity like illustrated in Fig. 4. Now the registration problem can be formulated as finding a transformation T that matches two corresponding 3D point sets. To ignore data that is not representing the investigated particle of interest, a SLIC superpixel segmentation[19] in combination with a DBSCAN clustering[20] is performed to detect the particle's contour. Additional thresholding and filling operations allow to create a particle mask. Due to the fact that the depth is computed from the rectified images that contain minor distortions and therefore differences in size and form, the wanted transformation needs to fix these deviations. It was experimentally validated that a rigid transformation[21] with only six degrees of freedom is not sufficient and results in a multilayered point cloud. Therefore an affine transformation T_a with twelve degrees of freedom was chosen that satisfies the equation

$$\begin{pmatrix} x_{B,i} \\ y_{B,i} \\ z_{B,i} \\ 1 \end{pmatrix} = \begin{pmatrix} a_{11} & a_{12} & a_{13} & a_{14} \\ a_{21} & a_{22} & a_{23} & a_{24} \\ a_{31} & a_{32} & a_{33} & a_{34} \\ 0 & 0 & 0 & 1 \end{pmatrix} \begin{pmatrix} x_{A,i} \\ y_{A,i} \\ z_{A,i} \\ 1 \end{pmatrix} . \tag{7}$$

Given two point sets P_A and P_B that consist of the homogeneous point vectors in Eq. (7), the equation can be solved in a least-squares sense for the affine transformation T_a using a Moore-Penrose pseudo inverse. As a last step T_a is applied to all points of the dense point cloud, the point set P_A was extracted from.

5. APPLICATION AND RESULTS

The investigated specimen illustrated in Fig. 3 consist of agglomerated diesel particulate matter. During the agglomeration process, irregular particle clusters are formed that have a high degree of complexity. For the 3D reconstruction process, stereo images with a tilt difference of 5° are captured, starting at a minimum tilt angle of -15° up to a maximum tilt angle of 30°. Between the left images of different stereo-pairs a difference of 10° is present, so that one tilt series between the minimum and maximum tilt angle results in five pairs of stereo images. Throughout the image acquisition of one tilt series, constant electron beam settings are used. Adjustments are carried out moving the stage along its x-,y- and z-axis to keep an explicit point in a pair of stereo images centered and the surface in focus range. For the obtained point clouds, meshs were created using a poisson reconstruction with constant parameters.[22]

Table 1. Absolute coordinate differences $[\Delta x\, \Delta y\, \Delta z]$ between the 3D point correspondences after the registration process.

Point sets	Mean difference [µm]	Max difference [µm]
15°/20° – 25°/30°	[0.091 0.059 0.508]	[0.475 0.272 4.779]
5°/10° – 15°/20°	[0.286 0.121 0.827]	[1.349 0.535 4.389]
-5°/0° – 5°/10°	[0.455 0.097 1.019]	[1.904 0.371 4.916]
-10°/-15° – -5°/0°	[0.468 0.045 0.738]	[2.202 0.170 3.461]

In Tab. 1 the remaining absolute coordinate differences between the 3D point correspondences of the different stereo images after the registration process are listed. The point set 25°/30° acts as the first fixed point cloud. After the transformation of the first moving point set 15°/20°, it takes the role of the next fixed one, repeating this procedure for the following point sets. It is noticeable that the error of the z-coordinate is much higher than the x-and y-differences. The explanation is that the x- and y-deviations consist of a small error caused by the feature matching and a higher error caused by the image distortions that result in different length ratios in the images. However, these errors are sufficiently corrected by the affine transformations. In contrary the differences of the z-coordinate are mainly caused by the reconstruction uncertainty of the depth h that is affected by the dense matching algorithm and the depth computation method described in Sec. 3.3. Nevertheless the noise of the point cloud's z-component remains bearable and is easily handled by the poisson surface reconstruction.

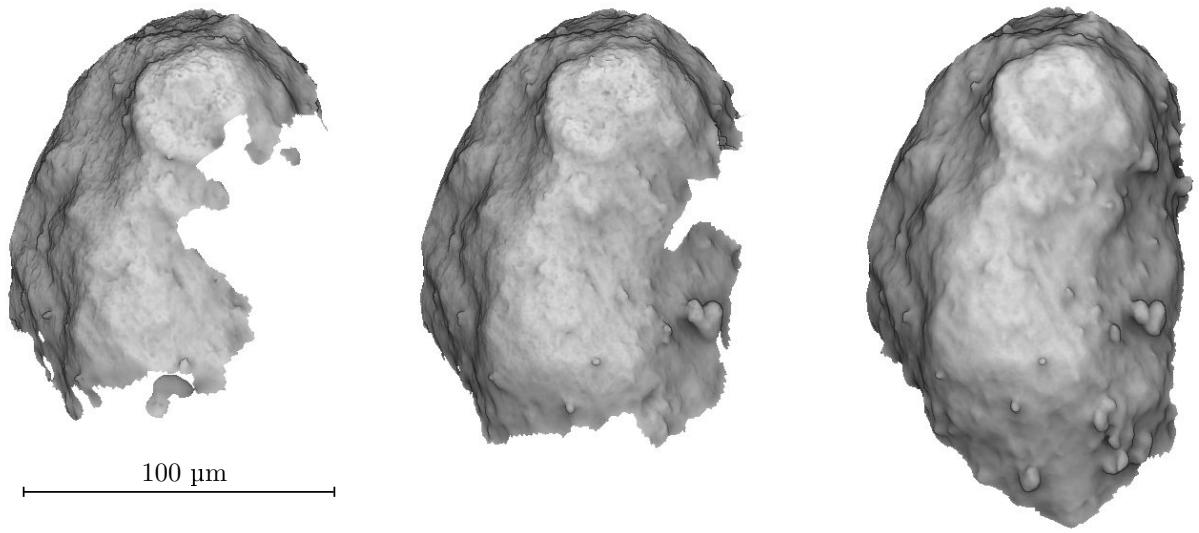

Figure 5. Correctly reconstructed mesh parts up to a chosen density (vertices per octree cell used for the poisson reconstruction) using one (left), three (middle) and all five (right) stereo images (starting with -15°/-10°).

The effect of combining the reconstructed 3D data from three and five stereo-pairs is demonstrated in Fig. 5. The shown meshs only contain parts up to a certain density of vertices per octree cell that was used in the poisson reconstruction process. When the point clouds are registered, besides the addition of missing data, a slight smoothing effect can be noticed that can be explained by the overall higher amount of vertices due to the overlapping parts between the stereo-pair images. The density of the final reconstructed mesh is illustrated by color in Fig. 6. It can be clearly seen that large vertical surface drops and overhanging structures still result in a low density of reconstructed vertices although the data from five stereo-pairs is combined. However, these critical parts can be easily improved using higher tilt angles and more images provided that a capable SEM stage is available.

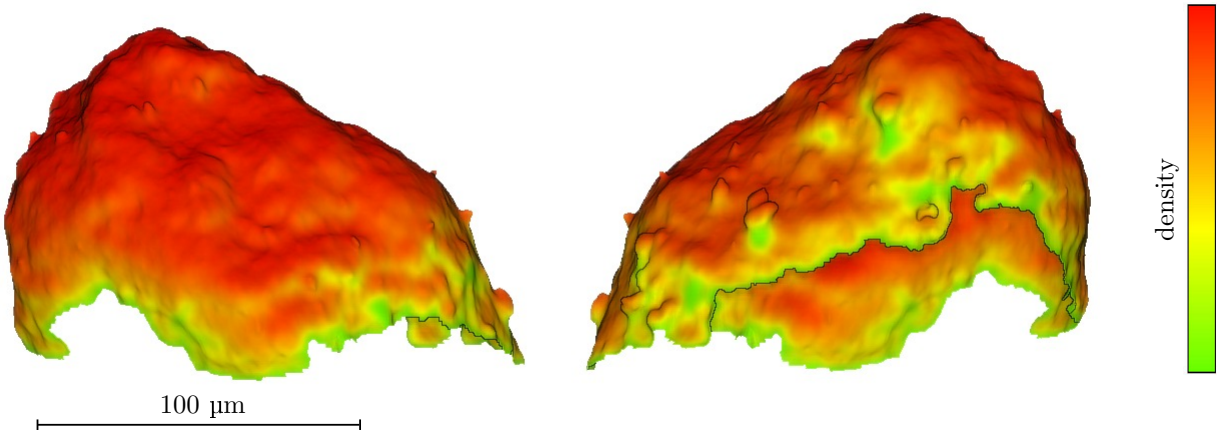

Figure 6. Generated mesh from the registered five point clouds illustrating the density of vertices per octree cell used for the poisson reconstruction by color (red indicates a high density and green indicates a low density).

6. CONCLUSION

The demonstrated method of registering point clouds from multiple stereo-pair images via point correspondences allows for the 3D reconstruction of objects with a large height-to-length ratio. Thereby problems that occur in scenarios where one stereo-pair is not sufficient to capture all wanted parts of an investigated specimen can be overcome. The obtained results are qualitative 3D measurements suitable for morphological analysis and visualization applications. The reconstruction scheme and the registration process works with uncalibrated stereo images and no knowledge about the camera poses of the SEM's virtual imaging system is required. By applying a SGBM algorithm to the rectified stereo images to perform a dense matching, occluded areas are marked, so that only valid pixel matches are used for the depth computation. The number of used stereo-pairs can be chosen arbitrarily and provided a capable SEM stage is available, the reconstruction quality of areas strongly occluded by overhanging surface structures can be increased adding more images taken with higher tilt angles. The illustrated results of the reconstructed particle agglomerates verify the method's functionality in difficult scenarios. In further works the dense reconstruction method could be combined with the determination of the camera poses and subsequent triangulation techniques to obtain a truly metric reconstruction result. An additional refinement of the local surface structure using shading information could additionally lead to an increase of surface details.

REFERENCES

[1] Joy, D. C. and Joy, C. S., "Low voltage scanning electron microscopy," *Micron* **27**(3-4), 247–263 (1996).

[2] Druckrey, A. M., Alshibli, K. A., and Al-Raoush, R. I., "3D characterization of sand particle-to-particle contact and morphology," *Computers and Geotechnics* **74**, 26–35 (2016).

[3] Miyamoto, A., Matsuse, H., and Koutaki, G., "Robust surface reconstruction by design-guided sem photometric stereo," *Measurement Science and Technology* **28**(4), 045405 (2017).

[4] Vynnyk, T., Scheuer, R., and Reithmeier, E., "3d-measurement using a scanning electron microscope with four everhart-thornley detectors," *Scanning Microscopies 2011: Advanced Microscopy Technologies for Defense, Homeland Security, Forensic, Life, Environmental, and Industrial Sciences* **8036**, 803615 (2011).

[5] Torr, P. H. and Zisserman, A., "Feature based methods for structure and motion estimation," *International workshop on vision algorithms* , 278–294 (1999).

[6] Xie, J., "Stereomicroscopy: 3d imaging and the third dimension measurement," *Application Note, Agilent Technologies* (2011).

[7] Baghaie, A., Tafti, A. P., Owen, H. A., D'Souza, R. M., and Yu, Z., "Three-dimensional reconstruction of highly complex microscopic samples using scanning electron microscopy and optical flow estimation," *PloS one* **12**(4), e0175078 (2017).

[8] Lowe, D., "Distinctive image features from scale-invariant keypoints," *International Journal of Computer Vision* **60**(2), 91–110 (2004).

[9] Alcantarilla, P. F., Bartoli, A., and Davison, A., "KAZE features," *European Conference on Computer Vision* , 214–227 (2012).

[10] Hartley, R. I., "In defence of the 8-point algorithm," *Fifth International Conference on Computer Vision* , 1064–1070 (1995).

[11] Fischler, M. A. and Bolles, R. C., "Random sample consensus: a paradigm for model fitting with applications to image analysis and automated cartography," *Communications of the ACM* **24**(6), 381–395 (1981).

[12] Hartley, R. and Zisserman, A., [*Multiple view geometry in computer vision*], Cambridge University Press (2003).

[13] Fathy, M. E., Hussein, A. S., and Toba, M. F., "Fundamental matrix estimation: A study of error criteria," *Pattern Recognition Letters* **32**(2), 383–391 (2011).

[14] Fusiello, A. and Irsara, L., "Quasi-euclidean epipolar rectification of uncalibrated images," *Machine Vision and Applications* **22**(4), 663–670 (2011).

[15] Hirschmueller, H., "Stereo processing by semiglobal matching and mutual information," *IEEE Transactions on pattern analysis and machine intelligence* **30**(2), 328–341 (2008).

[16] Birchfield, S. and Tomasi, C., "A pixel dissimilarity measure that is insensitive to image sampling," *IEEE Transactions on Pattern Analysis and Machine Intelligence* **20**(4), 401–406 (1998).

[17] Tomasi, C. and Manduchi, R., "Bilateral filtering for gray and color images," *IEEE Sixth International Conference on Computer Vision* , 839–846 (1998).

[18] Cui, L. and Marchand, E., "Calibration of scanning electron microscope using a multi-image non-linear minimization process," *IEEE International Conference on Robotics and Automation* , 5191–5196 (2014).

[19] Achanta, R., Shaji, A., Smith, K., Lucchi, A., Fua, P., and Süsstrunk, S., "SLIC superpixels compared to state-of-the-art superpixel methods," *IEEE transactions on pattern analysis and machine intelligence* **34**(11), 2274–2282 (2012).

[20] Ester, M., Kriegel, H. P., Sander, J., and Xu, X., "A density-based algorithm for discovering clusters in large spatial databases with noise," *Kdd* **96**(34), 226–231 (1996).

[21] Arun, K. S., Huang, T. S., and Blostein, S. D., "Least-squares fitting of two 3-D point sets," *IEEE Transactions on Pattern Analysis & Machine Intelligence* **5**, 698–700 (1987).

[22] Kazhdan, M. and Hugues, H., "Screened poisson surface reconstruction," *ACM Transactions on Graphics* **32**(3), 29 (2013).